JACS
JOURNAL OF THE AMERICAN CHEMICAL SOCIETY

ARTICLE

pubs.acs.org/JACS

Spectroscopic Detection of DNA Quadruplexes by Vibrational Circular Dichroism

Valery Andrushchenko,*[,†] Dimiter Tsankov,[‡] Maria Krasteva,[§] Helmut Wieser,[§] and Petr Bouř*[,†]

[†]Institute of Organic Chemistry and Biochemistry, Academy of Sciences of the Czech Republic, 16610 Prague, Czech Republic
[‡]Institute of Organic Chemistry, Bulgarian Academy of Sciences, BG-1113 Sofia, Bulgaria
[§]Department of Chemistry, University of Calgary, Calgary, Alberta, Canada T2N 1N4

Supporting Information

ABSTRACT: The four-stranded G-quadruplex motif is a conformation frequently adopted by guanine-rich nucleic acids that plays an important role in biology, medicine, and nanotechnology. Although vibrational spectroscopy has been widely used to investigate nucleic acid structure, association of particular spectral features with the quadruplex structure has to date been ambiguous. In this work, experimental IR absorption and vibrational circular dichroism (VCD) spectra of the model quadruplex systems $d(G)_8$ and deoxyguanosine-5′-monophosphate (5′-dGMP) were analyzed using molecular dynamics (MD) and quantum-chemical modeling. The experimental spectra were unambiguously assigned to the quadruplex DNA arrangement, and several IR and VCD bands related to this structural motif were determined. Involvement of MD in the modeling was essential for realistic simulation of the spectra. The VCD signal was found to be more sensitive to dynamical structural variations than the IR signal. The combination of the spectroscopic techniques with multiscale simulations provides extended information about nucleic acid conformations and their dynamics.

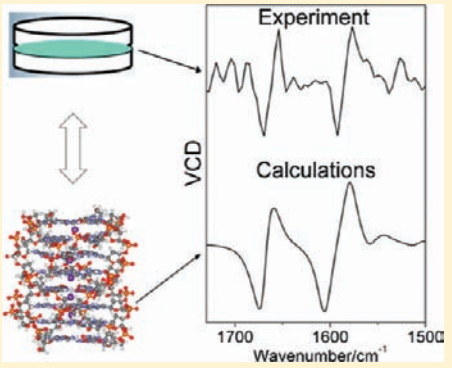

INTRODUCTION

Guanine-rich DNA and RNA, such as poly-G, can form various multiple-stranded structures. Their geometries can alter in time, which somewhat complicates spectroscopic characterization of these biopolymers in vitro.[1] One such structure is the G-quadruplex motif, which is based on four Hoogsteen-paired coplanar guanine bases.[2,3] The G-quadruplex structure can be formed both by guanine-rich oligo- or polynucleotides and by (deoxy)guanosine monophosphate (dGMP or GMP) monomers. In the former case, single-stranded oligomers assemble into four-stranded helices. In the latter case, GMP or dGMP molecules first assemble into G-quartet dimers, which further stack into columnar helical quadruplex structures.[3−5] Both structural types are stabilized by monovalent cations (usually K^+ or Na^+) present inside the quadruplex channel.

The G-quadruplex motif plays an important role in vivo,[2−4,6−9] and it has been found in telomeres[10] and other regions of the genome.[11−13] Ligands that bind specifically to the G-quadruplex regions in telomeres may inhibit telomerase activity in cancer cells and enable cancer cell proliferation control.[8,14−17]

Further applications of G-quadruplex structures have been suggested in the nanotechnology industry, such as their use in biosensors,[18,19] G-wires, G-quadruplex nanotubes, artificial synapses and ions channels, G-quadruplex nanomachines, and guanosine-based organic semiconductors.[3]

Vibrational spectroscopy has proven to be indispensable in structural and conformational studies of nucleic acids. Quadruplex characterization has been done with many techniques, including spectroscopic methods such as IR absorption[1,20−23] Raman,[24−26] and vibrational circular dichroism (VCD).[27−30] However, the association of the spectra with particular structures formed by guanine-rich oligonucleotides is often ambiguous because of the multitude of possible conformations and their alterations and interconversions with time.

An early IR study of poly-G structures suggested that they can exist in both metastable and stable forms, possibly of the quadruplex type, which are characterized by the carbonyl group absorption bands at 1695−1686 and 1674−1669 cm^{-1}, respectively.[1] The guanine ring absorption bands were identified at 1585 and 1589 cm^{-1}, respectively, for the two forms.[1]

In subsequent VCD studies of poly-G, the carbonyl absorption band was reported to appear at 1684[27] and 1688 cm^{-1}.[28] In the former work, the VCD feature appeared as a weak positive couplet, while in the latter, a positive band at 1675 cm^{-1} was observed. In both cases, the spectra were attributed to a multistranded (possibly quadruplex) poly-G conformation.

An intense carbonyl band and the corresponding positive VCD couplet at 1698 cm^{-1} were reported in the spectra of ordered single-stranded poly-G obtained by a heating/cooling procedure.[28] Alternatively, the IR carbonyl band of unordered, thermally denatured single-stranded poly-G was found at 1668 cm^{-1}.[1]

Received: May 20, 2011
Published: August 08, 2011

Another VCD study attributed IR spectra with a carbonyl band at 1682 cm^{-1} and a guanine ring band at 1585 cm^{-1} to a poly-G quadruplex structure.[29] A VCD couplet was observed only for the former band. The same study suggested a conversion of the G·G·G·G quadruplex into a G·G duplex upon heating or lowering of the pH to 3.1. The duplex structure was characterized by two features: (i) a carbonyl band with a strong VCD couplet at 1670 cm^{-1} and (ii) a strong guanine ring VCD couplet at 1589 cm^{-1}. The latter feature was considered the most prominent G·G duplex spectroscopic signature.

Recent IR and VCD studies of the deoxy-oligonucleotides $d(G)_{12}$ and $d(GGGA)_5$, which are capable of forming a quadruplex structure, resulted in quite different spectra.[23,30] Guzman et al.[23] identified the carbonyl band at 1692 cm^{-1} and the guanine ring band at 1588 cm^{-1}, while Nový et al.[30] observed these bands at 1670 and 1587 cm^{-1}, respectively. In the latter study, a weak positive carbonyl VCD couplet and a fairly strong negative guanine ring VCD band were also observed. Both authors ascribed their spectra to a quadruplex conformation.

Thus, G-quadruplex structures have been associated with a variety of vibrational spectra. Time-dependent spectral modifications have been attributed to either a "quadruplex metastable → quadruplex stable" transition or a "quadruplex → duplex" transition. In order to clarify this ambiguity and investigate in detail the spectra−structure relationship, we employed the IR and VCD spectroscopic techniques in combination with theoretical multiscale molecular dynamics (MD)/quantum-mechanical (QM) spectral modeling to investigate the structures formed by $d(G)_8$ octanucleotides and deoxyguanosine-5′-monophosphate (5′-dGMP) model systems. We used VCD spectroscopy because it provides richer information about the DNA structure, conformational changes, and intermolecular interactions than IR. It combines the advantages of good spectral resolution of the IR absorption with high structural sensitivity of the CD phenomenon.[31−35]

VCD spectra of nucleic acids have often been interpreted using semiempirical procedures such as the coupled oscillator model.[36−39] However, quantum-chemical computations enable a more universal assignment of experimental IR and VCD spectral features to the structure,[40,41] although they are restricted by the size of the investigated systems. Nevertheless, with the aid of the Cartesian coordinate tensor transfer (CCT) technique,[42] which was also used in the present study, quantum-chemical calculations can be extended to fairly large molecules, including nucleic acids.[43−46] As demonstrated below, the experiments and spectral simulations consistently designate IR and VCD spectral patterns characteristic of the G-quadruplex structure.

MATERIALS AND METHODS

Experimental Section. 2′-Deoxyguanosine-5′-monophosphate (5′-dGMP) was purchased from Sigma-Aldrich (Oakville, ON) and used without further purification. The $d(G)_8$ oligonucleotide was synthesized by University of Calgary Core DNA Services (Applied Biosystems Model 380B) using the standard phosphoramidite method. The crude product was desalted and purified by column chromatography using a column packed with Sephadex G-25. All salts were of ACS grade (Sigma-Aldrich) and used as supplied.

A Bomem MB100 spectrometer equipped with VCD optics and described elsewhere[47] was used for the spectral measurements. The concentration of the samples in the spectroscopic cell was 10 mM strand for $d(G)_8$ oligonucleotides and 0.3 M for dGMP. The samples were dissolved in D_2O containing either NaCl (60 mM to 0.8 M) or KCl (5 mM to 0.5 M) and buffered by 40 mM sodium cacodylate. The pH was varied from slightly acidic (pH 5.5) to neutral (pH 7.5) by dropwise addition of 0.1 N DCl or 0.1 N NaOD (or KOD). All samples were contained in a standard 25 μm BaF_2 cell (International Crystal Laboratories, Garfield, NJ) and maintained at 5 °C (unless stated otherwise) in a variable-temperature chamber. A circulating water thermostat (NESLAB Instruments, Portsmouth, NH) controlled with an accuracy of ±0.1 °C by a Cu−constantan thermocouple (OMEGA Engineering, Stanford, CT) was used to maintain the cell temperature. A total of 7500 ac scans (2 h 55 min scanning time) were accumulated and ratioed against 750 dc scans for the VCD spectra, while 750 dc scans were collected for the IR absorption spectra, all at a resolution of 4 cm^{-1}. The VCD spectra of all samples were corrected for absorption and polarization artifacts by subtracting the corresponding solvent VCD spectra taken under the same conditions.

Molecular Dynamics Simulations. The initial geometry of the $d(G)_8$ quadruplex was constructed using the NMR structure of the d(TTGGGGT) quadruplex[48] (PDB entry 139D) (Figure 1a,d). Single-stranded and duplex $d(G)_8$ structures were created from the quadruplex by removing three and two strands, respectively (Figure 1b,c).

The MD input preparation was done with the *xleap* module of the Amber 9 package.[49] All of the studied systems were neutralized with K^+ ions. For the quadruplex, seven ions were put inside the channel of the quadruplex and placed approximately equidistantly along the channel between the tetrad layers. The neutralized systems were then placed in an octahedral water box extending at least 10 Å in each direction from the DNA molecule (Figure 1a).

The MD simulations were performed with the *sander* module of Amber 9 using the parm99 force field with parmbsc0 refinement[50] for DNA and the TIP3P[51] force field for water. Three restrained minimizations were done to relax the initial geometry. Each stage consisted of 500 steepest-descent steps followed by 500 conjugate-gradient steps. In these stages, the DNA atoms were restrained using force constants of 80, 40, and 2 kcal mol^{-1} $Å^{-2}$, respectively. Next, an unrestrained minimization consisting of 1000 steepest-descent and 1500 conjugate-gradient steps was performed. Finally, the system was heated from 0 to 300 K for 20 ps while keeping the DNA atoms restrained using a force constant of 10 kcal mol^{-1} $Å^{-2}$. The unrestricted dynamics was started with 100 ps of equilibration and continued by a 20 ns production run, both at 300 K. A Langevin thermostat with the collision frequency $\gamma = 1$ and the SHAKE algorithm for the hydrogen atoms with a tolerance of 10^{-5} Å and a 2 fs time step were used for the equilibration and production stages. The particle-mesh Ewald (PME) method was employed to handle long-range electrostatic interactions, while Lennard-Jones interactions were cutoff at 10 Å.

The resulting MD trajectories were analyzed with the *ptraj* utility of Amber 9. Fourteen snapshot structures from the last 10 ns of the production run were randomly selected for the spectral modeling. The simulations were repeated at 278 K with nearly the same results.

Ab Initio Calculations of Spectral Parameters. To achieve feasible computational times, all of the octamer systems were split into smaller fragments [Figure S1 in the Supporting Information (SI)] for which the parameters important for spectral simulations could be obtained from accurate ab initio calculations. All of the fragments were subjected to quantum-chemical computations using the Gaussian 03 program package[52] without symmetry restrictions.

Smaller fragments, such as two stacked guanine bases $(\mathbf{G})_2$ (Figure S1), two stacked base pairs $(\mathbf{G2})_2$, and a base quartet **G4** as well as sugar−phosphate dimers $(\mathbf{SP})_2$ were optimized at the B3LYP[53]/6-31++G** approximation level, with the solvent modeled using COSMO.[54] In some cases, to speed up the computations, the geometry was preoptimized using the HF/6-31G** approximation in vacuum.

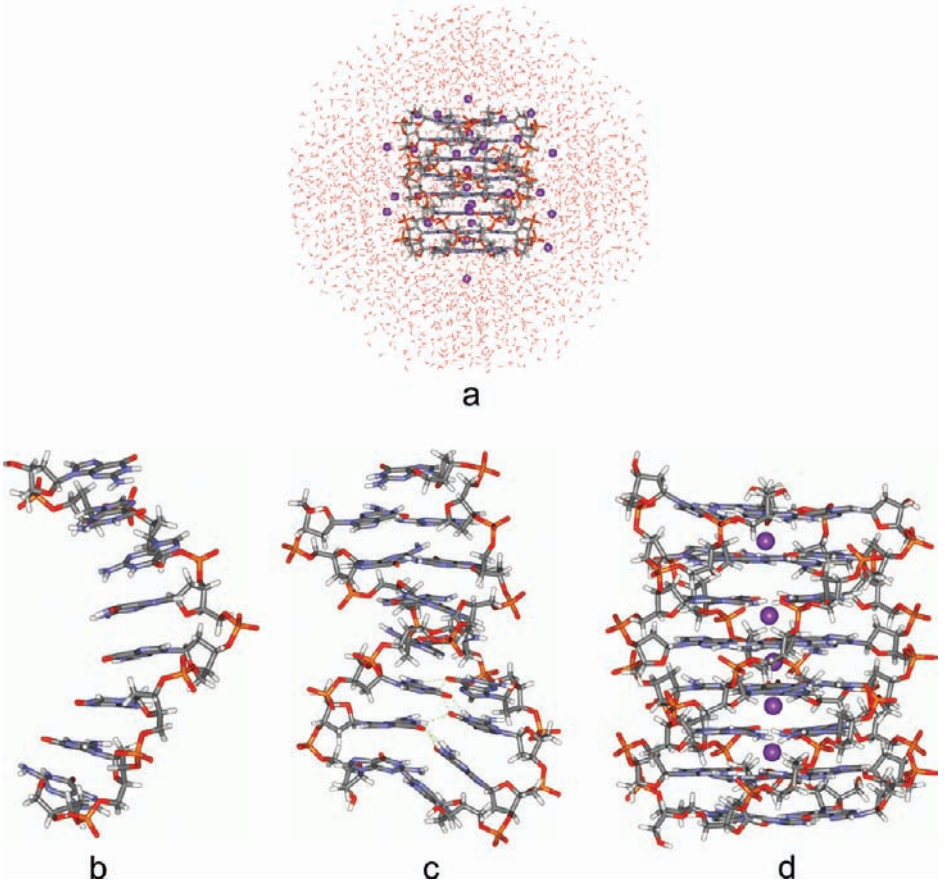

Figure 1. (a) Starting MD structure of the $d(G)_8$ solvated quadruplex and (b−d) the lowest-energy structures for (b) single-stranded, (c) duplex, and (d) quadruplex forms of $d(G)_8$. The K^+ ions are plotted as violet balls; in (b−d), water molecules and counterions have been removed for clarity.

For the larger fragments, namely, the full dimers of single-stranded, duplex, and quadruplex systems with the sugar−phosphate linkage [**d(G)$_2$**, **d(G2)$_2$**, and **d(G4)$_2$**, respectively (Figure S1)], the BPW91 functional[55,56] and 6-31G** basis set in vacuum were used. The B3LYP functional and the COSMO correction were not utilized in this case because of the large size of the systems (e.g., the quadruplex dimer has 274 atoms and 3198 basis functions). The BPW91 functional in vacuum produces vibrational frequencies close to those obtained using B3LYP with the implicit solvent, at least for the nitrogen base vibrational region.[44,45,57] The precision of the spectral simulation could be further increased using CCT method (see below), which enables one to combine the lower-level results for larger fragments with the more advanced computations on smaller fragments. Accounting for the dispersion interaction by the empirical Grimme correction[58] generally overestimated the interaction but did not significantly change the results for the quadruplex dimers (details of the test calculations are provided in the SI). Notably, unlike the duplex and single strands, the quadruplex structure is not primarily stabilized by dispersion and thus is less sensitive to this correction.

The sugar−phosphate dimers and the irregular full single-stranded, duplex, and quadruplex dimers were optimized only partially in order to preserve the geometry obtained from MD. The partial optimization was done in vibrational normal mode coordinates using the QGRAD program[59] interfaced to Gaussian 03, with modes having frequencies ω within (−300, 300 cm^{-1}) being frozen.

Finally, for all of the fragments, force field (FF) and atomic polar and axial tensors (APTs and AATs, respectively) were calculated at the same level of theory as used for the optimization.

Tensor Transfer and Generation of Spectra. The molecular property tensors (FF, APT, AAT) were transferred from the smaller fragments to the larger dimers and then from the dimers to the octamers using the CCT technique[42] (see the SI for details). The resultant harmonic FF was diagonalized, and the computed frequencies and intensities were used to simulate the IR absorption and VCD spectra of the octamers using 10 cm^{-1} wide Lorentzian bands.

In order to account for the dynamical effects and conformational flexibility of the system, the spectra were simulated for each of the 14 selected MD snapshots. Spectra of the snapshots were then averaged for each structure with equal weights.

RESULTS AND DISCUSSION

Experimental 5′-dGMP Spectra. Experimental IR absorption and VCD spectra of 5′-dGMP at 5 and 25 °C are plotted in Figure 2. The main structurally important absorption and VCD bands appear in two wavenumber regions, 1700−1500 and 1100−900 cm^{-1}, corresponding to the nitrogen base and sugar−phosphate moiety vibrations, respectively. Detailed assignments of these bands can be found elsewhere.[39,44,57,60−65]

The spectrum of 5′-dGMP at 5 °C exhibits the most intense VCD couplets at 1677(+)/1670(−) and 1599(+)/1588(−) cm^{-1}, arising from C═O stretching and guanine ring stretching/deformation vibrations at 1672 and 1596 cm^{-1}, respectively.[39,44,57,60] Several weaker sugar−phosphate VCD features are visible between 1100 and 900 cm^{-1}, although the noise level in this region is usually higher.

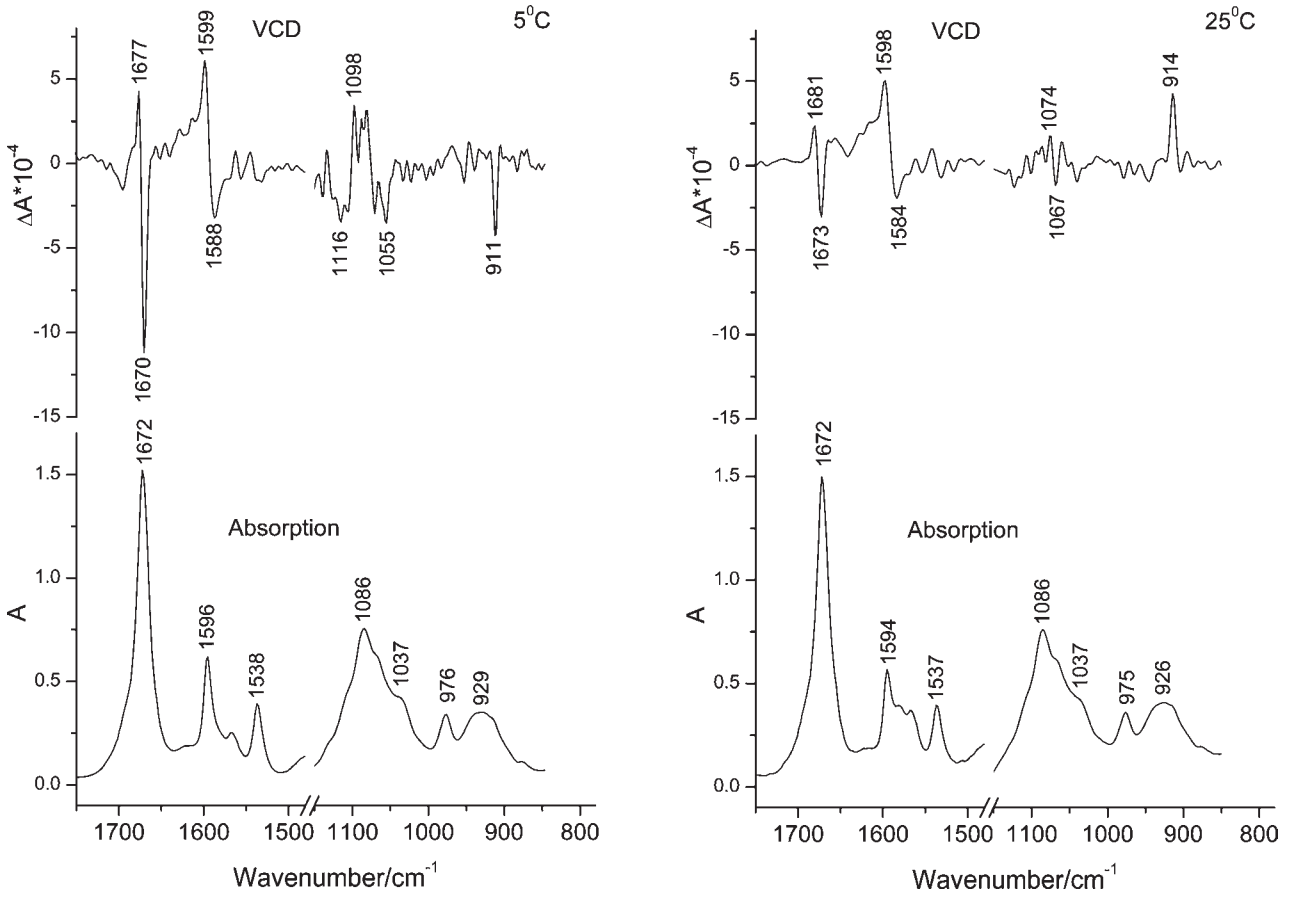

Figure 2. Typical experimental (bottom) IR absorption and (top) VCD spectra of 5′dGMP at (left) 5 and (right) 25 °C in the presence of K^+ ions at pH 5.5.

The strong VCD signal indicates an ordered helical orientation of the 5′-dGMP molecules, whereas a random orientation would not produce detectable VCD.[33,39,46,66] As can be seen in Figures S5−S7 in the SI, only spectra computed for the quadruplex conformation agree well with the experimental pattern. The spectra of stacked single-stranded and duplex structures deviate significantly from the experimental one. Similarly, neither of the computed spectra for the different G·G duplex arrangements (see the discussion below and Figure 7) is compatible with the measured data. It is thus reasonable to suppose that 5′-dGMP monomers form G-quartets that further self-assemble into columnar stacks to form G-quadruplexes, similar to structures revealed by X-ray crystallography.[5]

The IR absorption (Figure 2) also agrees well with the spectra of 5′-dGMP quadruplexes obtained by other authors: the C═O band at 1672−1680 cm^{-1}, the guanine base absorption at ∼1593 cm^{-1}, and the decreased intensity of the latter as a result of a hypochromic effect caused by the $\pi-\pi$ electron interaction of the stacked guanine rings.[20−23] A relatively strong guanine band at 1535−1537 cm^{-1} also indicates the formation of a helical structure.[1] Notably, monomeric 5′-dGMP exhibits very different IR spectra: the carbonyl band appears at 1663−1666 cm^{-1}, the guanine ring band has intensity comparable to the carbonyl and appears at 1575−1580 cm^{-1}, and the helical marker band at 1535−1537 cm^{-1} is weak.[21−23,57] Large differences between the IR spectra shown in Figure 2 and those for monomeric 5′-dGMP were also observed in the sugar−phosphate range.[57]

A right-handed DNA helix (e.g., A- or B-form) usually produces a positive carbonyl VCD couplet, while a left-handed helix (e.g., Z-form) produces a negative couplet.[31,46,67−69] The VCD spectra in Figure 2 show negative couplets; therefore, we can assume that the 5′-dGMP G-quadruplex is a left-handed helix. Other authors came to a similar conclusion on the basis of electronic CD (ECD) spectra of dGMP.[70,71]

There are rather minor differences in the 5′-dGMP IR spectra measured at 5 and 25 °C (Figure 2). The VCD, which is more sensitive to the temperature-induced structural changes, shows an overall intensity decrease. The most affected are the carbonyl couplet, whose amplitude diminishes by a factor of ∼4 at the higher temperature, and the sugar−phosphate VCD features, which decrease virtually to the noise level. The peak at 911 cm^{-1} even flips its sign and becomes positive at 25 °C. At the same time, the base deformation modes (1500−1600 cm^{-1}) do not change significantly. As the main VCD spectral features are conserved, we suppose that the quadruplex is still stable at the higher temperature but that the structure becomes less regular, which results in the overall decrease in the VCD signal. In particular, an overlap of the bases must still be present at 25 °C, which gives rise to the largely unchanged guanine ring VCD signal at ∼1590 cm^{-1}. On the other hand, an ordered arrangement of the polar carbonyl groups and sugar−phosphate moieties is affected more by the structural fluctuations and the solvent, resulting in significant decreases in the corresponding VCD intensities. This is in agreement with the exciton enhancement of VCD for regular DNA strands discussed previously.[72]

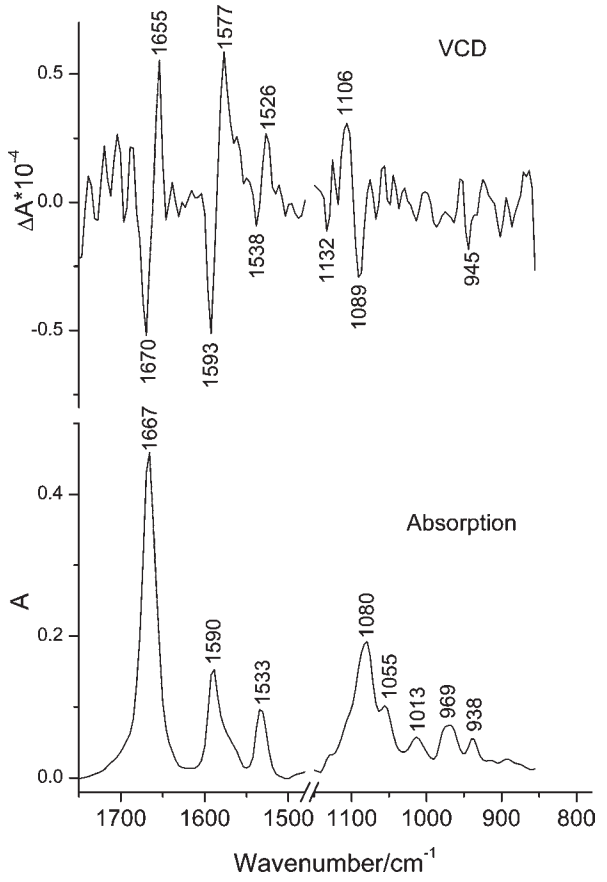

Figure 3. Typical experimental (bottom) IR absorption and (top) VCD spectra of $d(G)_8$ at 5 °C in the presence of K^+ ions at pH 5.5.

Experimental $d(G)_8$ Spectra. Despite the general similarity of the $d(G)_8$ spectra (Figure 3) to those of 5′-dGMP (Figure 2), there are a number of important differences. As in the case of dGMP, the most intense VCD couplets at 1670(−)/1655(+) and 1593(−)/1577(+) cm^{-1} arise from the C═O stretching and guanine base stretching/deformation vibrations at 1667 and 1590 cm^{-1}, respectively.[33,39,44,60−65] The well-defined VCD signal implies that the $d(G)_8$ strands form an ordered helical structure. However, the couplets have opposite sign in comparison with 5′-dGMP, suggesting a right-handed direction of the octamer helix. This is in agreement with the results of previous ECD studies on quadruplexes formed by guanine oligomers.[70] The distinct couplet at 1106(+)/1089(−) cm^{-1} arising from the symmetric phosphate vibrations at 1080 cm^{-1} indicates higher ordering of the phosphate groups in the octamer backbone relative to the not covalently linked and more flexible sugar−phosphate moieties in the 5′-dGMP assemblies.[33,39,44,60,69]

While the helical structure of $d(G)_8$ could be deduced from the experiment, it was not clear whether the spectra corresponded to a single-, double-, or multiple-stranded conformation, as mentioned in Introduction. In particular, the low wavenumber of the carbonyl band (1667 cm^{-1}, Figure 3) was intriguing, since this is normally characteristic of a monomeric, or single-stranded, or denatured structure, wherein hydrogen bonds are formed only with the solvent molecules, elongating the C═O bonds.[32,73] Single-stranded and both metastable and stable quadruplex structures of poly-G yielded higher wavenumbers for the carbonyl vibration.[1,28] On the other hand, the guanine ring band at 1590 cm^{-1} was observed in a stable quadruplex structure,[1,30] while the corresponding VCD couplet was assigned to a duplex.[29] Thus, to provide a rational interpretation of the experimental data, we performed MD simulations and used quantum-chemistry tools to calculate IR and VCD spectra for the single-stranded, duplex, and quadruplex $d(G)_8$ systems.

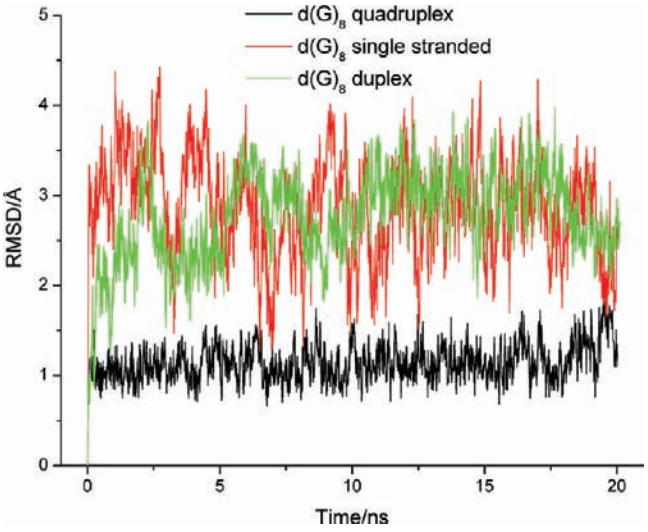

Figure 4. MD results for $d(G)_8$: rmsd's from the initial structure for quadruplex, duplex, and single-stranded forms.

Molecular Dynamics Simulations. The dependencies of the root-mean-square deviations (rmsd's) from the initial structures on time for single-, double-, and four-stranded $d(G)_8$ are shown in Figure 4. The plots indicate higher rigidity of the quadruplex relative to the other forms. The quadruplex geometry oscillates around an average structure with a low rmsd of ∼1 Å. Similar stability was observed previously in MD simulations of parallel-stranded G-quadruplexes.[74−76] The single-stranded and duplex structures are much more flexible, with rmsd's of ∼3.5 Å.

The variations in the distances between potassium ions as well as between neighboring guanine quartets in the quadruplex during the MD run are plotted in Figure 5. The largest structural fluctuations arise from terminal parts, particularly those lacking the stabilizing potassium ions, as follows from the quartet distance evolution (Figure 5 bottom). Some of the K^+ ions, which were initially placed in all vacant positions inside the quadruplex channel, changed location during the simulations. For example, two terminal ions (K1 and K7 in Figure 5) moved out from the channel, and one of the vacant positions was taken by the neighboring ion (K2 in Figure 5). Only the potassium ions in the middle of the quadruplex remained at their locations for the whole duration of the simulation. They are arranged approximately linearly and equidistantly separated from each other by ∼3.66 Å. Similar interionic distances were found experimentally (3.76 Å for Na^+ [77] and 3.4 Å for K^+ [78]). On a longer time scale, there is a dynamic equilibrium between the in-channel ions and free counterions or water molecules, particularly in the terminal regions of the quadruplex. The structure remains stable even with a few missing cations in the channel, in agreement with previous studies.[75]

The terminal fluctuations seen in the MD run reflect end-effect phenomena, which are common for ordered nucleic acid structures.[79] However, when the potassium ion is present, it

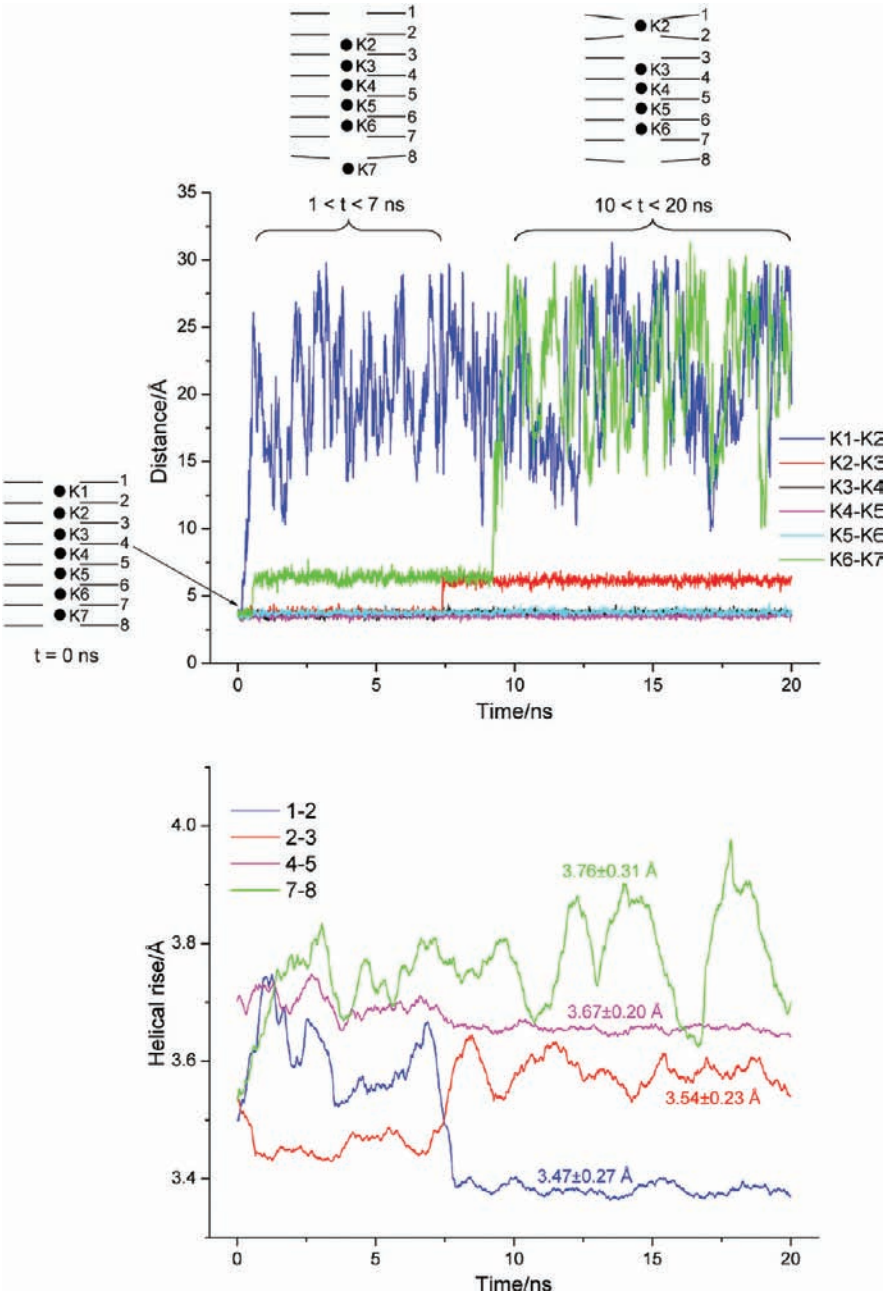

Figure 5. MD results for $d(G)_8$: time evolution of (top) the distances between the neighboring in-channel K^+ ions for the quadruplex and (bottom) the quadruplex interlayer distances (helix rise) between the neighboring guanine quartets. Schematic representations of the in-channel K^+ ions are shown for the top graph for times 0 ns, 1 ns < t < 7 ns, and 10 ns < t < 20 ns in the MD simulation; the ions are shown as black balls labeled K1 to K7, and the guanine quartet planes are shown as horizontal lines labeled 1 to 8. The same numbering of the quartet planes is used in the bottom panel. The average distance between stable ions is 3.7 ± 0.1 Å, and the overall average helical rise is 3.6 ± 0.1 Å.

reduces the end fraying (for example, the distance between quartets 1 and 2 varies less after an ion moves there) (Figure 5 bottom). The smallest fluctuations occur for the middle quartets, which are stabilized by K^+ from both sides. The calculated average helical rise of ~3.6 Å agrees reasonably well with the experimental rise of 3.2−3.6 Å,[78,80−83] and the value of 3.3 Å from previous MD simulations.[75] Lack of an ion in the channel may affect this value, inducing buckling of the quartet planes (see the schematic structure representations in Figure 5 and snapshot structure **c** in Figure 8), as is sometimes observed in NMR[48,84] and crystal structures.[85]

Unlike for the rise, there is no apparent correlation between presence of a K^+ ion or the end effects and the helical twist fluctuations (data not shown). However, the average twist angles are notably different for the central layers (35°) and the terminal tetrads (23−25°), indicating a partial unwinding of the helix at the ends. This is consistent with X-ray and NMR experimental data (30−37° and 20−25° for the inner and outer quartets, respectively).[80−83] The calculated average twist for the middle quartets (excluding the end effects) is ~30.5°, corresponding well to value of 30−31° derived from experiment.[77,80,81]

dx.doi.org/10.1021/ja204630k | *J. Am. Chem. Soc.* 2011, 133, 15055–15064

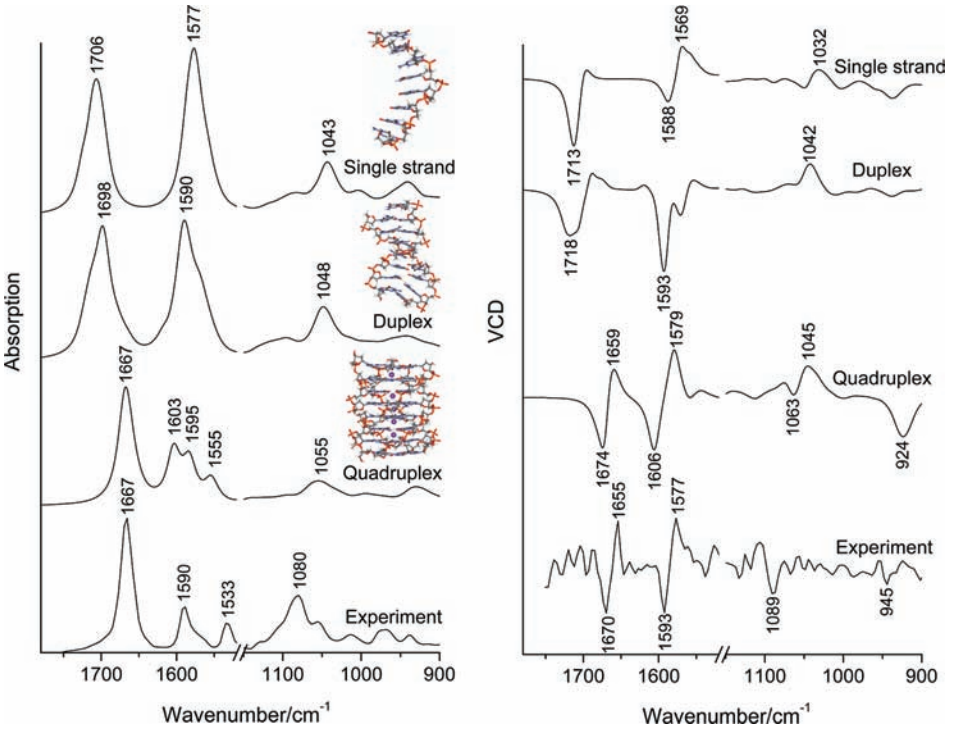

Figure 6. Experimental (left) IR absorption and (right) VCD spectra of $d(G)_8$ compared with the corresponding dynamically averaged computed spectra of single-stranded, duplex, and quadruplex structures. No scaling has been used for the computed spectra. The lowest-energy MD geometries are shown for each computational model. The violet balls in the quadruplex structure represent K^+ ions.

Table 1. Selected Calculated (for Single-Stranded, Duplex, and Quadruplex) and Experimental [for $d(G)_8$] IR Absorption and VCD Frequencies (cm^{-1}) and Their Assignments

single-stranded		duplex		quadruplex		$d(G)_8$ experiment		
IR	VCD	IR	VCD	IR	VCD	IR	VCD	assignment
1706	1713(−)	1698	1718(−)	1667	1674(−) /1659(+)	1667	1670(−) /1655(+)	ν(C6═O) (G)
1577	1588(−) /1569(+)	1590	1593(−)	1603, 1595	1606(−) /1579(+)	1590	1593(−) /1577(+)	ring def. (G)
–	–	1567(sh)[a]	1571(−)	1555	–	1533	–	ring def. (G)
1043	1032(+)	1048	1042(+)	1055	1063(−) /1045(+)	1080	1089(−)	ν(P═O) sym

[a] sh = shoulder.

Computed Spectra of Guanine Octamers. The calculated IR and VCD spectra of the single-stranded, duplex, and quadruplex octamers are compared to the experimental $d(G)_8$ spectra in Figure 6. The positions and assignments of the most intense peaks are summarized in Table 1. Clearly, in the nitrogen base vibrational region (1500−1700 cm^{-1}), the quadruplex model agrees with the experimental observations much better than the other two forms do. The wavenumber of the carbonyl IR band calculated for the quadruplex at 1667 cm^{-1} matches the experimental counterpart, while the duplex and single-stranded frequencies are too high. The low carbonyl wavenumber in both the experiment and the quadruplex computations can be explained by electrostatic attractions between carbonyl oxygens and potassium ions in the channel, which elongate the C═O bond to 1.26 Å (vs the value of 1.25 Å obtained in the test calculations for a canonical Watson−Crick G···C base pair). It should be noted that such a small difference in the bond length may well shift the vibrational frequency by 15−20 cm^{-1}.[86]

The computed guanine ring modes at 1603 and 1555 cm^{-1} can be assigned to the 1590 and 1533 cm^{-1} experimental absorptions; the band at 1595 cm^{-1} most probably corresponds to the experimental shoulder at ∼1570 cm^{-1}. The overall band shape is reproduced quite reasonably.

Even more apparent evidence for the quadruplex structure follows from the VCD spectra (Figure 6 right). The calculated quadruplex spectrum has two positive VCD couplets of similar amplitudes at 1674(−)/1659(+) and 1606(−)/1579(+) cm^{-1}, matching the experimental ones at 1670(−)/1655(+) and 1593(−)/1577(+) cm^{-1}. On the other hand, the VCD spectra calculated for the single-stranded and duplex octamers do not match the experiment so well. For example, the carbonyl vibration for the single-stranded structure shows only a negative band at 1713 cm^{-1} and the duplex has both VCD signatures negative, whereas nearly conservative couplets are present in the experimental spectrum.

The sugar−phosphate region is more difficult to analyze; nonetheless, the computed quadruplex spectra reproduce the

main experimental features in this range as well. The experimental absorption at 1080 cm^{-1} (Figure 6) assigned to symmetric P═O

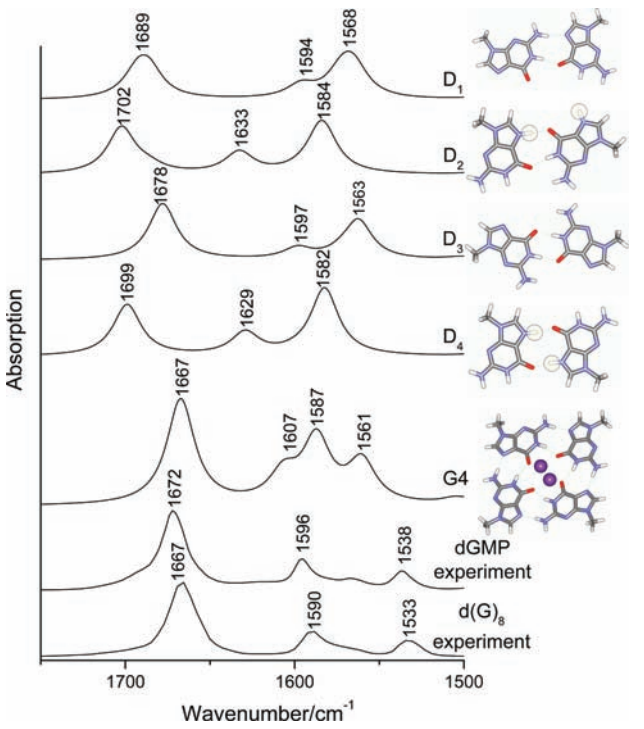

Figure 7. Calculated IR absorption spectra and corresponding structures of guanine G·G base pairs suggested in ref 29 compared with the calculated spectrum of the **G4** quartet and the experimental spectra of 5′-dGMP and $d(G)_8$. The designation of the base pairs is the same as in ref 29. It should be noted that D_2 and D_4 base pairs contain guanine species protonated at N7 position (highlighted by the circles). The violet balls in the **G4** structure represent K^+ ions.

vibrations[63,64] is calculated at 1055 cm^{-1} for the quadruplex, although its intensity is somewhat underestimated. As pointed out above, VCD analysis in this region is hampered by low signal-to-noise ratio in the experiment and a strong sugar−phosphate hydration for which the simulations can only partially account. Still, the negative experimental peaks at 1089 and 945 cm^{-1} can be attributed to the negative bands at 1063 and 924 cm^{-1} in the computed quadruplex spectrum, whereas the simulated single-stranded and duplex spectra differ much more from the experiment.

Overall, we can conclude that the simulations convincingly indicate that (i) the $d(G)_8$ system in the experiment adopts the quadruplex structure and (ii) the experimentally obtained spectral pattern is specific for the quadruplex.

G·G Duplex Simulation. A recent VCD study suggested that the G-quadruplex structure can disproportionate into a guanine duplex and that this process is facilitated by elevated temperature or low pH.[29] Several structural arrangements have been proposed for the guanine base pairs, including those with a protonated N7 site at low pH.[29] In order to provide further verification of our calculations for the octamers, we performed complete optimization and spectral modeling for all of the proposed duplex base pairs at the B3LYP/CPCM/6-31++G** level. The results are compared with the simulated spectra of the guanine quartet **G4** and the experimental spectra of 5′-dGMP and $d(G)_8$ in Figure 7.

As shown in Figure 7, none of the computed IR spectra of the base pairs D_1−D_4 correspond to the observations. All of the computational models provide incorrect intensity distributions for the guanine ring absorption around 1590 cm^{-1}. Except for pair D_3, the calculated carbonyl wavenumbers are too high (1689, 1702, 1678, and 1699 cm^{-1}, for D_1−D_4, respectively). The N7 protonation leads to an extra band at ∼1630 cm^{-1} that is not observed in our experimental spectra. On the other hand, the spectrum of the guanine base quartet **G4** closely matches the

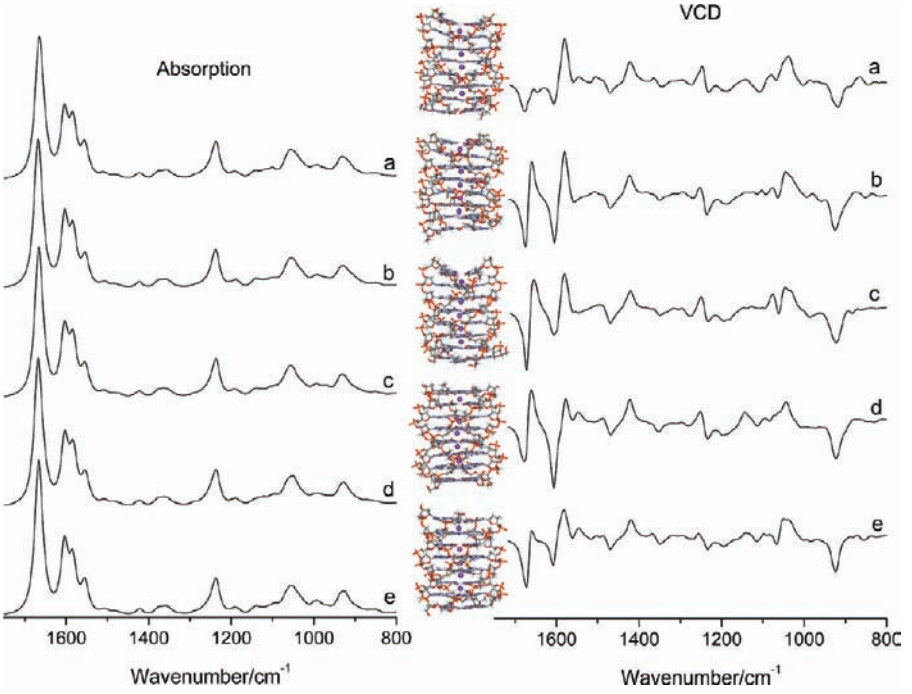

Figure 8. Computed (left) IR absorption and (right) VCD spectra of five random $d(G)_8$ quadruplex MD snapshot structures. The snapshot geometries are shown next to the corresponding VCD spectra. The violet balls represent K^+ ions.

observed spectra, confirming that the quadruplex structure is the most consistent with our experimental results.

Influence of the Quadruplex Flexibility on the Spectra. It was shown above that the calculated quadruplex spectra averaged over a number of MD snapshots and accounting for the dynamics of the system agreed well with experiment (Figure 6). Additionally, spectra computed for individual snapshot geometries can provide information on spectral sensitivity to thermal structural fluctuations. This was documented for five random snapshot structures and their corresponding IR and VCD spectra, as shown in Figure 8. While the IR spectra for different snapshots vary quite insignificantly, the VCD spectra change more substantially, indicating much higher sensitivity of the latter technique to minor structural variations. However, the basic VCD pattern remains stable and thus reflects the relatively high rigidity of the quadruplex geometry predicted by the MD simulations.

CONCLUSIONS

We studied solution conformations of the $d(G)_8$ and 5′-dGMP model systems and found that both adopt the quadruplex structure under our experimental conditions. This was confirmed by analysis of the IR and VCD spectra performed with the help of combined MD/QM modeling. The spectral simulations were based on the Cartesian tensor transfer routine, which provided results of nearly ab initio quality for the whole quadruplex system. From several arrangements of $d(G)_8$ (single-stranded, duplex, and quadruplex), only the quadruplex structure was fully compatible with the experimental observations. The MD simulations not only provided realistic geometries but also enabled the spectra from multiple snapshots to be averaged, thus improving the computed spectroscopic response by accounting for the dynamics of the system. VCD was found to be more sensitive to dynamical fluctuations of DNA geometry than IR. The obtained results show that vibrational spectroscopic techniques coupled with advanced simulations can be conveniently used to identify the conformations of nucleic acids and other large biopolymers.

ASSOCIATED CONTENT

Supporting Information. Details of the fragmentation of the DNA geometries for ab initio computations (Figure S1); details of the CCT procedure (Figures S2 and S3); effect of the implicit solvent on the computed spectra (Figure S4); effect of Grimme's dispersion correction on the dimer structure and spectra (Figures S5−S7); and complete refs 49 and 52. This material is available free of charge via the Internet at http://pubs.acs.org.

AUTHOR INFORMATION

Corresponding Author
andrushchenko@uochb.cas.cz; bour@uochb.cas.cz

ACKNOWLEDGMENT

The work was supported by the Grant Agency of the Czech Republic (Grants P208/10/0559 to V.A. and P208/11/0105 to P.B.); the Academy of Sciences (Grant M200550902 to P.B.); the Ministry of Education, Youth and Sports (Grant LH11033 to P.B.); and the Natural Sciences and Engineering Research Council of Canada (H.W.). The authors thank Dr. Zuzana Vokáčová for the help with the MD simulations and Dr. Marie Urbanová and Dr. Iryna Goncharova for the test ECD measurements.

REFERENCES

(1) Howard, F. B.; Frazier, J.; Miles, H. T. *Biopolymers* **1977**, *16*, 791–809.
(2) Gellert, M.; Lipsett, M. N.; Davies, D. R. *Proc. Natl. Acad. Sci. U.S.A.* **1962**, *48*, 2013–2018.
(3) Davis, J. T. *Angew. Chem, Int. Ed.* **2004**, *43*, 668–698.
(4) Gottarelli, G.; Spada, G. P.; Garbesi, A. In *Comprehensive Supramolecular Chemistry*; Lehn, J.-M., Atwood, J. L., MacNicol, D. D., Davies, J. A. D., Vögtle, F., Sauvage, J.-P., Housseini, M. W., Eds.; Pergamon: Oxford, U.K., 1996; Vol. 9.
(5) Forman, S. L.; Fettinger, J. C.; Pieraccini, S.; Gottarelli, G.; Davis, J. T. *J. Am. Chem. Soc.* **2000**, *122*, 4060–4067.
(6) Simonsson, T. *Biol. Chem.* **2001**, *382*, 621–628.
(7) Keniry, M. A. *Biopolymers* **2000**, *56*, 123–146.
(8) Han, H. Y.; Hurley, L. H. *Trends Pharmacol. Sci.* **2000**, *21*, 136–142.
(9) Burge, S.; Parkinson, G. N.; Hazel, P.; Todd, A. K.; Neidle, S. *Nucleic Acids Res.* **2006**, *34*, 5402–5415.
(10) Blackburn, E. H. *Cell* **1994**, *77*, 621–623.
(11) Kilpatrick, M. W.; Torri, A.; Kang, D. S.; Engler, J. A.; Wells, R. D. *J. Biol. Chem.* **1986**, *261*, 1350–1354.
(12) Sen, D.; Gilbert, W. *Nature* **1988**, *334*, 364–366.
(13) Simonsson, T.; Pecinka, P.; Kubista, M. *Nucleic Acids Res.* **1998**, *26*, 1167–1172.
(14) Neidle, S.; Read, M. A. *Biopolymers* **2000**, *56*, 195–208.
(15) Helder, M. N.; Wisman, G. B.; van der Zee, G. J. *Cancer Invest.* **2002**, *20*, 82–101.
(16) Huppert, J. L. *Philos. Trans. R. Soc., A* **2007**, *365*, 2969–2984.
(17) Oganesian, L.; Bryan, T. M. *BioEssays* **2007**, *29*, 155–165.
(18) Ueyama, H.; Takagi, M.; Takenaka, S. *J. Am. Chem. Soc.* **2002**, *124*, 14286–14287.
(19) Alberti, P.; Mergny, J. L. *Proc. Natl. Acad. Sci. U.S.A.* **2003**, *100*, 1569–1573.
(20) Miles, H. T.; Frazier, J. *Biochim. Biophys. Acta* **1964**, *79*, 216–220.
(21) Howard, F. B.; Miles, H. T. *J. Biol. Chem.* **1965**, *240*, 801–805.
(22) Miles, H. T.; Frazier, J. *Biochem. Biophys. Res. Commun.* **1972**, *49*, 199–204.
(23) Guzman, M. R.; Liquier, J.; Brahmachari, S. K.; Taillandier, E. *Spectrochim. Acta, Part A* **2006**, *64*, 495–503.
(24) Gramlich, V.; Klump, H.; Herbeck, R.; Schmid, E. D. *FEBS Lett.* **1976**, *69*, 15–18.
(25) Simard, C.; Savoie, R. *Biopolymers* **1994**, *34*, 91–100.
(26) Miura, T.; Thomas, G. J. *Biochemistry* **1995**, *34*, 9645–9654.
(27) Annamalai, A.; Keiderling, T. A. *J. Am. Chem. Soc.* **1987**, *109*, 3125–3132.
(28) Xiang, T.; Goss, D. J.; Diem, M. *Biophys. J.* **1993**, *65*, 1255–1261.
(29) Petrovic, A. G.; Polavarapu, P. L. *J. Phys. Chem. B* **2008**, *112*, 2245–2254.
(30) Nový, J.; Böhm, S.; Králová, J.; Král, V.; Urbanová, M. *Biopolymers* **2008**, *89*, 144–152.
(31) Andrushchenko, V. V.; van de Sande, J. H.; Wieser, H.; Kornilova, S. V.; Blagoi, Y. P. *J. Biomol. Struct. Dyn.* **1999**, *17*, 545–560.
(32) Andrushchenko, V.; Blagoi, Y.; van de Sande, J. H.; Wieser, H. *J. Biomol. Struct. Dyn.* **2002**, *19*, 889–906.
(33) Andrushchenko, V.; Tsankov, D.; Wieser, H. *J. Mol. Struct.* **2003**, *661*, 541–560.
(34) Polyanichko, A. M.; Andrushchenko, V. V.; Chikhirzhina, E. V.; Vorob'ev, V. I.; Wieser, H. *Nucleic Acids Res.* **2004**, *32*, 989–996.
(35) Tsankov, D.; Krasteva, M.; Andrushchenko, V.; van de Sande, J. H.; Wieser, H. *Biophys. Chem.* **2006**, *119*, 1–6.
(36) Zhong, W. X.; Gulotta, M.; Goss, D. J.; Diem, M. *Biochemistry* **1990**, *29*, 7485–7491.

(37) Zhong, W. X.; Gulotta, M. S.; Goss, D. J.; Diem, M. *Biophys. J.* **1990**, *57*, A457–A457.
(38) Wang, L.; Keiderling, T. A. *Biochemistry* **1992**, *31*, 10265–10271.
(39) Keiderling, T. A. In *Circular Dichroism and the Conformational Analysis of Biomolecules*; Fasman, G. D., Ed.; Plenum Press: New York, 1996; pp 555−597.
(40) Stephens, P. J.; Devlin, F. J.; Gasparrini, F.; Ciogli, A.; Spinelli, D.; Cosimelli, B. *J. Org. Chem.* **2007**, *72*, 4707–4715.
(41) Freedman, T. B.; Cao, X. L.; Dukor, R. K.; Nafie, L. A. *Chirality* **2003**, *15*, 743–758.
(42) Bouř, P.; Sopková, J.; Bednárová, L.; Maloň, P.; Keiderling, T. A. *J. Comput. Chem.* **1997**, *18*, 646–659.
(43) Andrushchenko, V.; Bouř, P. *Chirality* **2010**, *22*, E96–E114.
(44) Bouř, P.; Andrushchenko, V.; Kabeláč, M.; Maharaj, V.; Wieser, H. *J. Phys. Chem. B* **2005**, *109*, 20579–20587.
(45) Andrushchenko, V.; Wieser, H.; Bouř, P. *J. Phys. Chem. B* **2004**, *108*, 3899–3911.
(46) Andrushchenko, V.; Wieser, H.; Bouř, P. *J. Phys. Chem. B* **2002**, *106*, 12623–12634.
(47) Tsankov, D.; Eggimann, T.; Wieser, H. *Appl. Spectrosc.* **1995**, *49*, 132–138.
(48) Wang, Y.; Patel, D. J. *J. Mol. Biol.* **1993**, *234*, 1171–1183.
(49) Case, D. A.; et al. *AMBER 9*; University of California: San Francisco, 2006.
(50) Perez, A.; Marchan, I.; Svozil, D.; Šponer, J.; Cheatham, T. E.; Laughton, C. A.; Orozco, M. *Biophys. J.* **2007**, *92*, 3817–3829.
(51) Jorgensen, W. L.; Chandrasekhar, J.; Madura, J. D.; Impey, R. W.; Klein, M. L. *J. Chem. Phys.* **1983**, *79*, 926–935.
(52) Frisch, M. J.; et al. *Gaussian 03*, revision D.02; Gaussian, Inc.: Wallingford, CT, 2004.
(53) Becke, A. D. *J. Chem. Phys.* **1993**, *98*, 1372–1377.
(54) Klamt, A.; Jonas, V.; Burger, T.; Lohrentz, J. C. W. *J. Phys. Chem. A* **1998**, *102*, 5074–5085.
(55) Perdew, J. P.; Wang, Y. *Phys. Rev. B* **1992**, *45*, 13244–13249.
(56) Becke, A. D. *Phys. Rev. A* **1988**, *38*, 3098–3100.
(57) Andrushchenko, V.; Bouř, P. *J. Phys. Chem. B* **2009**, *113*, 283–291.
(58) Grimme, S. *J. Comput. Chem.* **2006**, *27*, 1787–1799.
(59) Bouř, P.; Keiderling, T. A. *J. Chem. Phys.* **2002**, *117*, 4126–4132.
(60) Andrushchenko, V.; Leonenko, Z.; Cramb, D.; van de Sande, J. H.; Wieser, H. *Biopolymers* **2001**, *61*, 243–260.
(61) Tsuboi, M.; Kyogoku, Y.; Shimanouchi, T. *Biochim. Biophys. Acta* **1962**, *55*, 1–12.
(62) Tsuboi, M. *Appl. Spectrosc. Rev.* **1969**, *3*, 45–90.
(63) Tsuboi, M. In *Basic Principles in Nucleic Acid Chemistry*; Ts'o, P. O. P., Ed.; Academic Press: New York, 1974; Vol. 1, pp 399−452.
(64) Taillandier, E.; Liquier, J.; Taboury, J. A. *Adv. Infrared Raman Spectrosc.* **1985**, *12*, 65–114.
(65) Theophanides, T.; Tajmir-Riahi, H. A. In *Spectroscopy of Biological Molecules*; Sandorfy, C., Theophanides, T., Eds.; Reidel: Dordrecht, The Netherlands, 1984; pp 137−152.
(66) Birke, S. S.; Diem, M. *Biophys. J.* **1995**, *68*, 1045–1049.
(67) Gulotta, M.; Goss, D. J.; Diem, M. *Biopolymers* **1989**, *28*, 2047–2058.
(68) Wang, L.; Keiderling, T. A. *Nucleic Acids Res.* **1993**, *21*, 4127–4132.
(69) Wang, L.; Yang, L.; Keiderling, T. A. *Biophys. J.* **1994**, *67*, 2460–2467.
(70) Bonazzi, S.; Capobianco, M.; Demorais, M. M.; Garbesi, A.; Gottarelli, G.; Mariani, P.; Bossi, M. G. P.; Spada, G. P.; Tondelli, L. *J. Am. Chem. Soc.* **1991**, *113*, 5809–5816.
(71) Gottarelli, G.; Proni, G.; Spada, G. P. *Enantiomer* **1996**, *1*, 201–209.
(72) Andrushchenko, V.; Bouř, P. *J. Comput. Chem.* **2008**, *29*, 2693–2703.
(73) Andrushchenko, V.; van de Sande, J. H.; Wieser, H. *Biopolymers* **2003**, *69*, 529–545.
(74) Špačková, N.; Berger, I.; Šponer, J. *J. Am. Chem. Soc.* **1999**, *121*, 5519–5534.
(75) Chowdhury, S.; Bansal, M. *J. Phys. Chem. B* **2001**, *105*, 7572–7578.
(76) Štefl, R.; Cheatham, T. E.; Špačková, N.; Fadrna, E.; Berger, I.; Koca, J.; Šponer, J. *Biophys. J.* **2003**, *85*, 1787–1804.
(77) Phillips, K.; Dauter, Z.; Murchie, A. I. H.; Lilley, D. M. J.; Luisi, B. *J. Mol. Biol.* **1997**, *273*, 171–182.
(78) Haider, S.; Parkinson, G. N.; Neidle, S. *J. Mol. Biol.* **2002**, *320*, 189–200.
(79) Saenger, W. *Principles of Nucleic Acid Structure*; Springer-Verlag: New York, 1984.
(80) Arnott, S.; Chandras., R.; Marttila, C. M. *Biochem. J.* **1974**, *141*, 537–543.
(81) Patel, P. K.; Hosur, R. V. *Nucleic Acids Res.* **1999**, *27*, 2457–2464.
(82) Schultze, P.; Smith, F. W.; Feigon, J. *Structure* **1994**, *2*, 221–233.
(83) Keniry, M. A.; Strahan, G. D.; Owen, E. A.; Shafer, R. H. *Eur. J. Biochem.* **1995**, *233*, 631–643.
(84) Aboulela, F.; Murchie, A. I. H.; Norman, D. G.; Lilley, D. M. J. *J. Mol. Biol.* **1994**, *243*, 458–471.
(85) Hazel, P.; Parkinson, G. N.; Neidle, S. *J. Am. Chem. Soc.* **2006**, *128*, 5480–5487.
(86) Callender, R.; Deng, H. *Annu. Rev. Biophys. Biomol. Struct.* **1994**, *23*, 215–245.